ADVANCED OPTICAL MATERIALS
www.advopticalmat.de

Direct Emission of Continuously Varying Polarization of Light by Surface Treatment of a Mesogenic Luminophore

Young-Kyo Seo, You-Jin Lee, Jae-Hoon Kim, and Chang-Jae Yu**

Control of the polarized light generated from a luminophore has been intensively studied in organic light emitting diodes due to an enhancement of light intensity. The direct emission of highly circularly polarized light has been reported in a twist stacking of an achiral conjugated polymer by boundary surface effect without any chiral dopant. Although the twisted configuration of the emitting layer was obtained by applying different boundary conditions to two interfaces of the conjugated polymer, little study has been performed on the effect of the interfaces of the mesogenic polymer so far. Here, twist-angle-varying configuration in a single luminophore is designed and demonstrated to investigate an interfacial effect such as surface anchoring phenomena of conjugated mesogenic polymer. The continuously varying twisted configuration is fabricated by applying the circularly and unidirectionally rubbing method to the lower and the upper interfaces of the mesogenic luminophore, respectively. The surface anchoring and bulk elastic properties of luminophores are systematically analyzed to investigate twist deformation. Furthermore, a self-luminous light source generating continuously varying polarization of light is demonstrated. The proposed light source can generate multi-polarization states including linearly polarized, right-handed circularly polarized, and left-handed circularly polarized light in a single substrate.

1. Introduction

Polarized light has been widely utilized in various applications such as improving the efficiency as well as reducing the glare of displays.[1–4] In particular, the emission of circularly polarized (CP) light has attracted significant attention in displays, optical components, and sensors.[5–8] In organic light-emitting diodes, the direct emission of CP light is obtained by chirality of a luminophore[9–13] or by the macroscopic configuration such as light propagating through a twist stacking of birefringence materials.[14,15] Especially, to obtain a highly polarized CP emission, the twist stacking of the mesogenic conjugated polymer was used, where one of the requirements for generating CP light was that the luminescent layer should contain chiral properties.[15] However, such approaches are only able to generate CP light with single-handedness in the entire luminescent layer since they contain a chiral part in the luminescent layer. An alternative approach was studied by Baek et al., in which they suggested a direct CP emitting process by introducing twisted deformation through the different surface treatments into the upper and lower interfaces of a luminophore.[16] The twist deformation is attained by controlling the boundary conditions of the emitting layer (EML) with a liquid crystalline (LC) phase due to its elasticity.[16–18] Here, the stable twist configuration is achieved by balancing between the elastic energy of the EML and the anchoring energy on the interfaces of the EML.[17,18] Thus, investigation of polymer anchoring energy is essential to analyze the twist deformation structure for the CP emission. However, little study has been performed on the effect of the interfaces of the mesogenic polymer so far.[12,13]

In this paper, we induced twist angles varying continuously along the EML area in a single substrate with the first circular and second unidirectional rubbing processes to investigate the surface boundary effect on the twist angle. We introduced a simple model for the distribution of twisted molecules based on the elastic and anchoring properties of the mesogenic conjugated polymer to analyze CP emission in the photoluminescence (PL) process. The twist angles were examined by analyzing the light propagating in the continuously twisted birefringent layers theoretically and calculating the degree of CP emission from the twist structure.[15,19] The degree of CP is defined as the dissymmetry factor, $g = 2(I_L - I_R)/(I_L + I_R)$, where I_L and I_R designate the intensities of left-handed (LH) and right-handed (RH) CP emission, respectively. From such analysis, the surface anchoring energy in the second rubbed interface was evaluated and we confirmed that the anchoring energies even in different thicknesses of the EML were coincident with each other since the interfacial phenomenon in the second rubbed interface was independent of the bulk EML region. Furthermore, we designed a multi-polarization light source that emits simultaneously or separately linearly polarized (LP), LHCP, and RHCP light on a single luminophore, which could generate multiple polarized lights along the EML area in the electroluminescence (EL) process.

Y.-K. Seo, Dr. Y.-J. Lee, Prof. J.-H. Kim, Prof. C.-J. Yu
Department of Electronic Engineering
Hanyang University
Seoul 04763, Korea
E-mail: jhoon@hanyang.ac.kr; cjyu@hanyang.ac.kr

The ORCID identification number(s) for the author(s) of this article can be found under https://doi.org/10.1002/adom.202002020.

DOI: 10.1002/adom.202002020

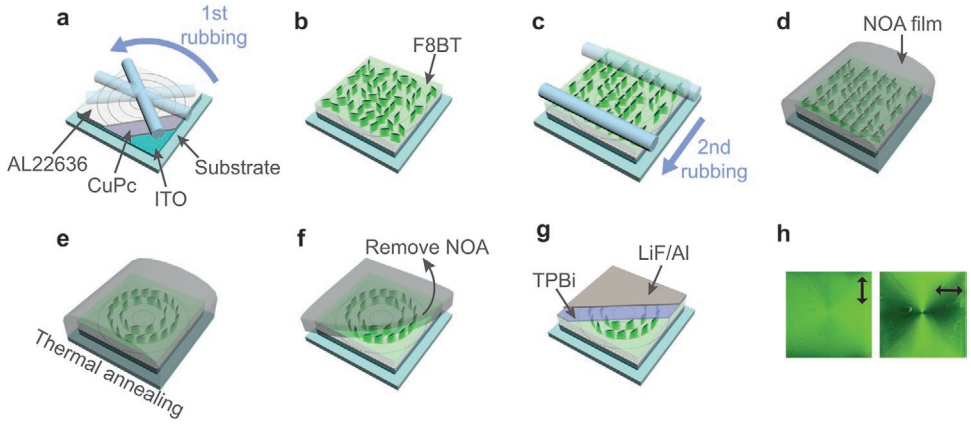

Figure 1. Schematic diagrams for the fabrication methods. a) The first circular rubbing on alignment layer (AL22636) as an electron blocking layer. b) Spin coating of the F8BT layer. c) Rubbing of the F8BT surface unidirectionally (the second rubbing). d) Spin coating of the UV epoxy (NOA) film on the rubbed F8BT layer and UV exposure for curing. e) Thermal annealing above mesogenic temperature of F8BT (180 °C). f) Slow cooling and removal of the NOA film. g) Thermal deposition of TPBi, LiF, and Al sequentially in a vacuum for the EL process. h) PL textures under linear polarizer. The arrows indicate the transmission axis of the polarizer. In left texture, the transmission axis of the polarizer is parallel to the second unidirectionally rubbing direction.

2. Results and Discussion

The fabrication process is schematically shown in **Figure 1**. Poly(9,9-di-n-octylfluorenyl-2,7-diyl)-alt-(benzo[2,1,3]thiadiazol-4,8-diyl) (F8BT) was used as the EML. To determine the lower surface boundary condition of the F8BT circularly (the first rubbing process), the substrate was spun while in contact with a fixed rubbing bar covered with cotton cloth (Figure 1a). The F8BT was spin coated on the circularly rubbed PI layer (Figure 1b). Two F8BT layers with 100 and 200 nm thicknesses were prepared. To establish the upper surface boundary condition (the second rubbing process), the F8BT itself was rubbed unidirectionally with a rubbing machine (Figure 1c). Thereafter, UV epoxy (NOA) was spin-coated on the F8BT surface and cured by exposure to UV light (Figure 1d). The cured resin acts as a protecting film to maintain the upper boundary condition after thermal annealing.[16] Then, thermal annealing of the F8BT above its mesogenic temperature to produce a continuous twist structure due to the elastic properties of the mesogenic polymer (Figure 1e). After cooling slowly to room temperature, the epoxy film was removed (Figure 1f). 2,2′,2″-(1,3,5-benzinetriyl)-tris(1-phenyl-1-H-benzimidazole) (TPBi) (20 nm), LiF (1 nm), and Al (70 nm) were sequentially deposited for the EL cell by thermal evaporation as a hole blocking layer (HBL), electron injection layer (EIL), and cathode, respectively (Figure 1g). The PL textures of the sample under the polarizer are shown in Figure 1h. In the PL textures, the dark section under the linear polarizer indicates that an orthogonal LP light to polarizer is emitted. The schematic diagram of the device structure and energy levels of the used materials shows in Figure S1, Supporting Information.

The alignment layer exhibits strong anchoring energy through the rubbing method at the first rubbing interface, and the aligned F8BT emits LP light with a high degree of linear polarization ratio along the rubbing direction.[20–23] On the other hand, the F8BT that rubbed itself at the second rubbing interface was aligned relatively weakly. As shown in Figure S2, Supporting Information, the degree of polarization ratio in the F8BT film aligned unidirectionally by the rubbed alignment layer was greater than that by the rubbed F8BT itself. Therefore, the first surface was aligned strongly by circular rubbing (the first rubbing condition) and the second surface was aligned relatively weakly by unidirectional rubbing of the F8BT itself (the second rubbing condition).

The continuously twisted structure is induced in the different rubbing directions in two rubbing surfaces due to the elastic properties of the mesogenic polymer under the fixed boundary conditions.[16] Such twist deformation is well-known in conventional LC displays (LCDs) with different anchoring strengths on the upper and lower surfaces.[24] As shown in **Figure 2**a, the red and blue arrows indicate the alignment direction of the first (circularly rubbing) and the second (unidirectionally rubbing) surfaces of the F8BT, respectively. Also, the section along the circularly rubbing direction can be defined by the rubbing angle of the substrate. In a stage of sample preparation, the rubbing angle is generally defined as an angle difference from the rubbing direction at the bottom (the second rubbing direction because the cathode is placed to the bottom side when the sample is observed) to the rubbing direction at the top surfaces (the first rubbing direction). Now, the rubbing angle matches to angle difference between the head of a red arrow and the head of a blue arrow in Figure 2a. Consequentially, the rubbing angle is varied from 0° to 360° representing a horizontal axis in Figure 2b. Since the two-fold symmetry of the F8BT and its high elasticity, that is, because of no differentiation between head and tail of the arrows of the rubbing direction, mesogenic molecules tend to twist in a direction leading to a smaller angle difference to minimize the energy of twist deformation. Therefore, the rubbing angle conducting a boundary condition should be defined as the energetically preferred rubbing angle ($|R_\theta| < 90°$) as shown in Figure 2a. For example, the rubbing angles from 0° to 90° are equivalent to the (energetically) preferred rubbing angles. However, in the case of the rubbing angles from 90° to 180°, the preferred rubbing

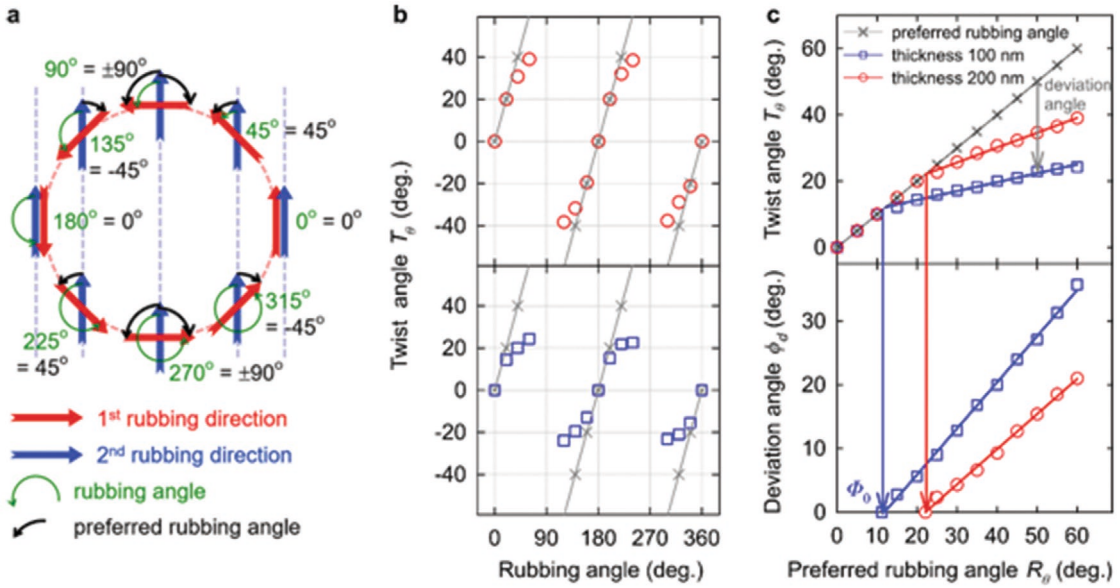

Figure 2. a) Schematic diagram of the rubbing direction in the sample along the position in the substrate and the relationship between the rubbing angle and the preferred rubbing angle energetically. The red and blue arrows represent the first circularly and the second unidirectionally rubbing directions, respectively. b) Actual twist angle of the F8BT layer measured at the rubbing angle. c) The twist angle (T_θ) and the deviation angle ($\phi_d = R_\theta - T_\theta$) as a function of the preferred rubbing angle (R_θ). Open squares (blue) and open circles (red) represent the measured twist angles from the F8BT layers with thicknesses of 100 and 200 nm, respectively. Cross symbols denote the energetically preferred rubbing angle in (b) and (c). The blue and red solid lines are linearly fitted for the measured twist angles as a function of the preferred rubbing angle. The slopes of the linear fits for the deviation angles are fitted to be 0.72 and 0.55 at the 100- and 200-nm-thick F8BT layers, respectively.

angle is reversed and decreased from 90° to 0° with increasing the rubbing angle. In this range, the preferred rubbing angle is denoted as a negative sign. Cross symbols present the preferred rubbing angle in Figure 2b,c.

The boundary condition conducted by the preferred rubbing angle generates a twisted structure in the EML, where the CP light is emitted in accordance with the twist angle of the EML.[15,16] The twist angle of the F8BT generated by the boundary condition was estimated from the Stokes parameters, passing through the continuously twisted F8BT layer of the incident probing light with linear polarization.[25] The calculated Stokes parameters as a function of the twist angle were compared to the measured Stokes parameters and then the twist angle was determined as shown in Figure S3, Supporting Information.

Figure 2b shows the measured twist angle in the entire rubbing angle and the corresponding preferred rubbing angle denoted by cross symbols. As shown in Figure 2b, the twist angle (T_θ) was increased and saturated at a certain critical angle with increasing the preferred rubbing angle (R_θ) due to competition between the bulk elastic and the surface anchoring energies of the F8BT and its high elasticity. When the surface anchoring strength is less than the elastic strength, an undesigned twist angle is achieved, although the continuous twist structure is induced from the lower to upper surface due to the elasticity of the F8BT.

To understand such twisted behavior quantitatively, we started the elastic continuum theory used in the statics of LCs for understanding their deformations.[18] In a bounded LC sample faced to two solid surfaces, the total energy (F_T) consists of the elastic deformation energy for bulk region (F_b) and two surface energies of the first and the second surface anchoring energies (F_s and F_s') as follows:[18,26]

$$F_T = F_b + F_s + F_s' \tag{1}$$

In our case, the elastic deformation energy comes only from the twist deformation energy, which is defined as a product of a twist elastic constant (K_2) and a square of the angle variation rate to the sample thickness as follow; $F_b = K_2(T_\theta)^2/(2d)$, where T_θ and d present the twist angle and the sample thickness, respectively.[18] The surface energy is generally expressed as a product of a surface anchoring strength (W and W') and a square of the sine function for the deviation angle from the preferred rubbing direction as follow; $F_s = W\sin^2(\phi_0)/2$ at the first rubbing surface and, $F_s' = W'\sin^2(\phi_d)/2$ at the second rubbing surface, where W and W' denote surface anchoring strength at each surface, and ϕ_0 and ϕ_d present the deviation angles from the preferred rubbing directions at each surface.[18,26] Note that the F8BT polymer faced to the alignment layer (the first rubbing surface) exhibits a better aligning property than that faced to the NOA layer (the second rubbing surface) as shown in Figure S2, Supporting Information. That is, W is stronger than W' and ϕ_0 is smaller than ϕ_d since the mesogenic molecules tend to be aligned along the rubbing direction at the stronger anchoring surface to minimize the total energy. For simplification, we assume that $\phi_0 = 0$.[27] Finally, the total energy consists of the elastic deformation energy (F_b) and the surface energy (F_S') at the second rubbing surface. In such twist deformation, the energetically stable configuration of the

mesogenic molecules comes from the competition and balance between the elastic restoring torque ($T_b = K_2 T_\theta / d$), and the surface anchoring torque ($T_s = W' \sin(2\phi_d)/2$). It should be noted that sum of the actual twist angle (T_θ) and the deviated angle in the second rubbing surface (ϕ_d) is the preferred rubbing angle (R_θ).

In the case of $T_s > T_b$, the mesogenic molecules tend to be aligned along the rubbing direction at the surface without deviation angle from the preferred rubbing direction. Therefore, the mesogenic molecules are continuously twisted from the first rubbing direction to the second one. That is, the twist angle (T_θ) is equivalent to the preferred rubbing angle (R_θ). Note that the elastic torque (T_b) is continuously increased with increasing the preferred rubbing angle and the surface torque is a constant because of no deviation angle until the elastic torque overcomes the surface torque.

On the other hand, in the case of $T_s < T_b$, the mesogenic molecules cannot be twisted up to the preferred rubbing angle since the elastic restoring torque is stronger than the surface anchoring torque. Therefore, as shown in Figure 2c, the twist angle (T_θ) is smaller than the preferred rubbing angle (R_θ) above a certain critical angle (Φ_0), which is determined by the condition that $T_s = T_b$. Now, we can express the surface anchoring energy as the constant surface energy in the case of $T_s > T_b$ and the additional surface anchoring energy, expressed as by the deviation angle such that $\phi_d \neq 0$ in the case of $T_s < T_b$. Simply, we can simply express the surface torque as follow; $T_s = W'(1 + \sin(2\phi_d))/2$. Now, at $T_s = T_b$ ($\phi_d = 0$), we can directly obtain the surface anchoring energy W' since $T_\theta = \Phi_0$, expressed as follows:

$$W' = \frac{2K_2 \times \Phi_0}{d} \tag{2}$$

The critical angles were determined to be 12.18° and 22.08° for 100- and 200-nm-thick F8BT films, respectively. By applying the twist elastic constant of the LC polymer ($K_2 \approx 10^{-10}$ to 10^{-11} N),[21,22] the surface anchoring energy can be evaluated from Equation (2) as $\approx 3.86 \times 10^{-5}$ to 3.86×10^{-4} Jm^{-2}, which is less than the anchoring strength of conventional LCDs alignment layers as expected.

To obtain the deviation angle ϕ_d in the regime of $T_s < T_b$, we minimized the total energy by ϕ_d after applying $\phi_d = R_\theta - T_\theta$ to Equation (1). After calculating $\partial F_T / \partial \phi_d = 0$, we can achieve a relationship between the preferred rubbing angle and the deviation angle as follows:

$$R_\theta = \frac{d \times W'}{2K_2} \sin(2\phi_d) + \phi_d \tag{3}$$

By considering approximately $\sin(2\phi_d) \approx 2\phi_d$, Equation (3) is expressed as follows:

$$\phi_d = \frac{1}{\frac{d \times W'}{K_2} + 1}(R_\theta) \tag{4}$$

Also, this equation can be rewritten as follows:

$$\phi_d = \frac{1}{2\Phi_0 + 1}(R_\theta) \tag{5}$$

As you know, the deviation angle is linearly proportional to the preferred rubbing angle. Finally, the slopes in Figure 2c (ϕ_d versus R_θ) were fitted to be 0.70 and 0.56 in the thicknesses of 100 and 200 nm F8BT films, respectively. Considering the thickness d in Equation (4), the surface anchoring energies W' are consistent with that evaluated in Equation (2).

We also investigate emission of the polarized light including the CP light from the continuously varying twist angles. To characterizing the CP light, the dissymmetric g factor was evaluated from the spectral intensities under LH and RH circular polarizer consisting of a linear polarizer and a quarter-wave plate (QWP) at 546 nm. **Figure 3** shows the dissymmetry factor g_{PL} at 546 nm in the PL process as a function of the twist angle for the 100 nm (Figure 3a) and the 200 nm (Figure 3b) thick F8BT layers (see Figure S4, Supporting Information). Note that the g_{PL} increases up to 2 with increasing the degree of LHCP but decreases down to −2 with increasing the degree of RHCP. Also, the zero g_{PL} means the LP light. Here, symbols depict the experimentally measured values and solid lines represent

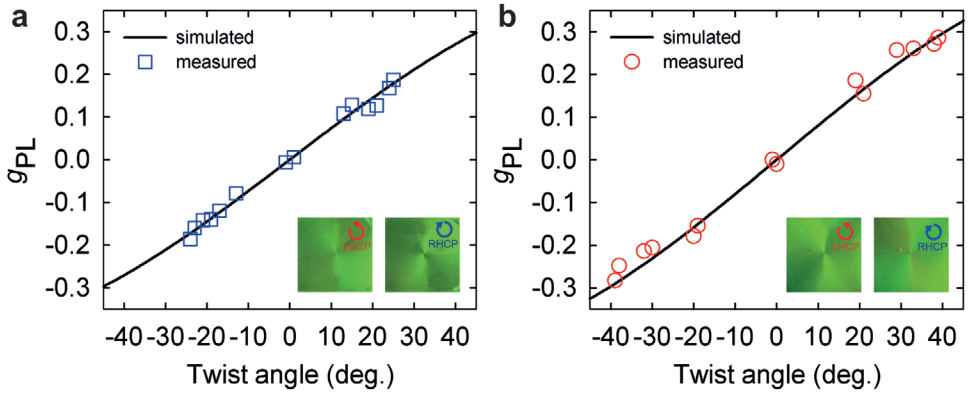

Figure 3. The dissymmetric factor g_{PL} as a function of twist angle (T_θ) for the F8BT layer with thicknesses of a) 100 and b) 200 nm. The symbols are the experimentally measured values from the CPPL and the solid line is the calculated value using the Müller matrix analysis. Inset PL textures were taken under the LH and RH circular polarizer.

the theoretically calculated ones, evaluated from the Müller matrix analysis for the twisted birefringent substance (Müller matrix analysis of PL process in Supporting Information and the works of Baek et al.[16] and Jung et al.[19] for details). For calculation, we assumed that the F8BT layer is divided into N sublayers, uniformly twisted, and each sublayer emits LP light.[16,19] It is evident from the results that the elliptical polarized light is caused as the LP light passes through the twisted layer and experiences phase retardation.[15] Here, because each sublayer is not aligned perfectly, they emit partially LP light (Figure S2, Supporting Information and the work of Baek et al.[16]). As shown in Figure 3, the measured g_{PL} is consistent with the calculated value regardless of the F8BT thickness. Note that we directly apply all parameters such as thickness, birefringence, twist angle, and degree of linear polarization obtained independently to our model without any fitting parameters, and calculate the g_{PL} factors as a function of the twist angle. Since the dissymmetric factor could be measured in a circularly dichroic medium, we measured the circular dichroism (CD) of the twisted F8BT (Figure S5, Supporting Information). Although the experimental CD signal is the sum of various contribution such as an isotropic CD and a macroscopic anisotropic CD,[28] its contribution to the g_{PL} is not significant. As a result, we confirmed that the dissymmetric factor was originated from the twisted structure, and continuously varying polarization of light including different-handedness CP light was emitted in a single substrate without any chiral agents. The inset images in Figure 3 indicate the PL textures under RH and LH circular polarizer. In the PL textures, the contrast in brightness under the circular polarizer implies emission of different CP light. From the LHCP light emitted in the leftward twist-inducing area (positive twist angles) to the RHCP light emitted in the rightward twist-inducing area (negative twist angles), continuously varying polarization states of light were implemented in a single luminophore.

Based on the study in PL process, we substantiated applicability of an EL device with continuous multi-polarization in a single substrate using a circular and unidirectional rubbing method. **Figure 4**a–c shows the measured CPEL spectra by inducing various twist angles with a 200 nm thick F8BT in a single substrate. In the region induced as $T_\theta = 0°$, LP light was emitted with no difference in LHCP and RHCP light intensity

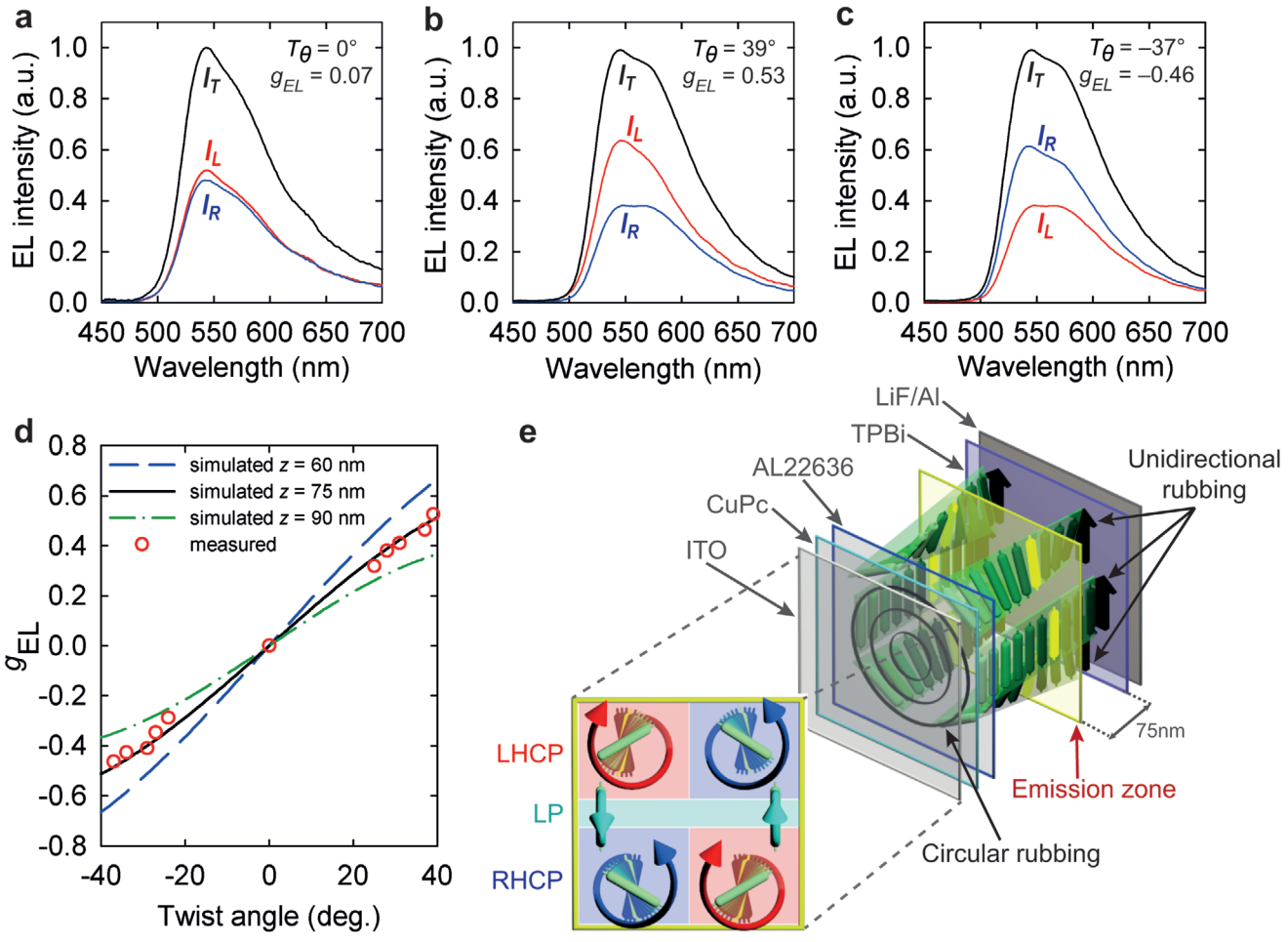

Figure 4. The EL spectra at different twist angles of a) $T_\theta = 0°$, b) $T_\theta = 39°$, and c) $T_\theta = -37°$. The EL spectra measured under no polarizer, and under LH and RH circular polarizers are depicted by the black (I_T), red (I_L), and blue (I_R) solid lines, respectively. d) The g_{EL} as a function of the twist angle. Symbols represent the g_{EL} values measured experimentally and the lines depict the g_{EL}'s simulated with Müller matrix analysis at various emission zones of distances (z) from the TPBi layer. e) Schematic structure of the light source generating multi-polarization states in a single EML.

(Figure 4a). In the region of $T_\theta = 39°$ induced by the preferred rubbing angle of $R_\theta = 60°$, LHCP light was emitted with a dissymmetry factor of $g_{EL} = 0.53$ (Figure 4b). Similarly, in the region of $T_\theta = -37°$ induced by the preferred rubbing angle of $R_\theta = -60°$, RHCP light was emitted with $g_{EL} = -0.46$ (Figure 4c). The g_{EL} factors for various twist angles including both leftward (positive twist angle) and rightward (positive twist angle) twisting areas are shown in Figure 4d.

In an EL device, to analyze the dissymmetric g_{EL} factor, emission zone (electron–hole recombination zone) is an essential parameter, which affects the optical and electrical properties.[29,30] To estimate the emission zone, we applied all parameters, used in the PL process, except for the emission zone to the EL model and calculated the g_{EL} factors as a function of the twist angle varying the emission zone as shown in Figure 4d. For simulation, we designated a specific sublayer (emission zone) emitting LP light, which passes through twisted birefringent sublayers ($\Delta n = 0.67$ at wavelength of 546 nm). Here, the LP light emitted from the emission zone proceeds simultaneously to the anode and the cathode. In particular, the LP light propagated toward the cathode is reflected from the cathode and experienced by all the twisted sublayers of the EML (Müller matrix analysis of EL process in Supporting Information and the works of Albano et al.[11] and Frédéric et al.[13] for further details). For simplifying the calculation, we ignore the interlayer and cavity effects such as light absorption, reflection, and scattering during light propagation.[31] Finally, we estimate that the emission zone is placed at about 75 nm from the TPBi layer (black solid line) after applying least-square-error as shown in Figure 4d. Consequently, we can confirm the location of the emission zone in the EML, which is consistent with the results of the EL device analysis fabricated under the same conditions.[16] As illustrated in Figure 4e, the light source generating continuously varying polarized light, including the LP, LHCP, and RHCP, in a single luminophore was implemented with the simple method using the circular and unidirectional rubbings.

Based on our analysis model for the EL devices, we also estimate the g_{EL} factor of the CP light emitted at z = 75 nm as a function of reflectance of the metal electrode (Figure S7, Supporting Information). The g_{EL} factor is increased with increasing reflectance of the Al metal (that is, increasing the thickness of the Al metal) since the reflected light from the electrode experiences phase retardation passing through entire twisted birefringent layers. The efficiency of the CPEL device with multi-polarized emission is measured to be 0.12 cd A^{-1} (see Figure S8, Supporting Information), which is smaller than that of the sample fabricated with unidirectionally rubbing method in both the bottom and top interfaces of the F8BT reported previously[16] since the circularly rubbing process was manually carried out.

3. Conclusion

In summary, the light source generating multi-polarization states in a single luminophore was demonstrated through the continuously varying twist structure of achiral conjugated polymer induced by the circular and unidirectional rubbings to its lower and upper surfaces. The continuously varying twist structure was achieved in disparate rubbing directions on the lower and upper surfaces of the mesogenic conjugated polymer due to its elasticity. We systematically investigated the relationship between the designed rubbing angle and the actual twist angle, and thus theoretically evaluated the anchoring strength based on the torque balance model in the twisted LC molecule. In addition, the varying twist angles were verified by comparing the experimentally measured and the theoretically calculated dissymmetry factors in the PL process. From analysis of the dissymmetry factor, the emissive light source with multi-polarization states including LP, LHCP, and RHCP light in a single luminophore was implemented by applying simple surface treatments. Our study not only provides a foundation for the anchoring properties of luminophores with mesogenic phases, but also suggests applicability to self-luminous light sources with multi-polarization such as polarization generating and controlling devices without light loss.

4. Experimental Section

Materials: As an emitting layer, the LC conjugate polymer of F8BT (from Sigma Aldrich) was dissolved in toluene for spin coating. F8BT has a nematic phase over 160 °C. Copper phthalocyanine (CuPc from Lumtec), 2,2′,2″-(1,3,5-benzinetriyl)-tris(1-phenyl-1-H-benzimidazole) (TPBi from Lumtec), LiF (from Lumtec), and Al (From iNexus Inc.) were used for HIL, HBL, EIL, cathode, respectively for EL cell.

Fabrication of EL Devices: CuPc was deposited by high-vacuum (6×10^{-6} torr) thermal evaporation on prepatterned indium tin oxide (ITO). For uniform alignment of the F8BT, polyimide (PI, AL22636) was spin coated on the CuPc and baked 210 °C for 60 min. The thicknesses of the CuPc and PI were 2 and 20 nm, respectively. The dissolved F8BT was spin coated at 1000 rpm for 10 s and 3000 rpm for 20 s on the circularly rubbed PI. The F8BT layer was unidirectionally rubbed with a rubbing machine (RMS-50-M from Nam Il Optical Instruments Co.). The machine has a 6.5 cm diameter roller covered with cotton cloth which fiber lengths and the number of fibers were 1.8 mm and 3750 fibers $inch^{-2}$, respectively. Next, an ultra-violet (UV) curable epoxy (NOA 68 from Norland Products Inc.) was covered the F8BT layer and cured by UV exposure for 25 min. The NOA layer was peeled off after thermal annealing at 180 °C for 10 min. Finally, TPBi, LiF, and Al were sequentially deposited by high-vacuum (6×10^{-6} torr) thermal evaporation. In the case of the PL process, it was fabricated without a cathode and other supporting layers. All processes were carried out inside a glove box with a N_2 atmosphere to avoid oxygen and humidity.

Measurement: For PL, a UV light source (365 nm) was used with an intensity 1000 W. The EL device was adjusted by applying voltages in 25 V in order to generate consistent intensity of the emitted light. The CP emission spectra were collected under the circular polarizer consisted with a linear polarizer and a QWP at 546 nm using a spectrometer (SR-UL-1R from TOPCON). All measured values of the *g* factors in the PL and EL processes were measured at 546 nm. The twist angle was determined by direct measurement of the Stokes parameters of the transmitted light,[18] and see Supporting Information for details.

Supporting Information

Supporting Information is available from the Wiley Online Library or from the author.

Acknowledgements

The authors acknowledge a National Research Foundation (NRF) of Korea for funding. C.J.Y. was supported by NRF of Korea (No. NRF-2018R1A2A3075276).

Conflict of Interest

The authors declare no conflict of interest.

Data Availability Statement

Research data are not shared.

Keywords

anchoring strength, mesogenic conjugated polymers, multi-polarization light sources, polarized emission, surface treatment

Received: November 24, 2020
Revised: February 4, 2021
Published online: March 16, 2021

[1] E. Matioli, S. Brinkley, K. M. Kelchner, Y.-L. Hu, S. Nakamura, S. DenBaars, J. Speck, C. Weisbuch, *Light: Sci. Appl.* **2012**, *1*, e22.
[2] B. Park, Y. H. Huh, H. G. Jeon, *Opt. Express* **2010**, *18*, 19824.
[3] D. W. Zhang, M. Li, C. F. Chen, *Chem. Soc. Rev.* **2020**, *49*, 1331.
[4] G. Albano, G. Pescitelli, L. D. Bari, *Chem. Rev.* **2020**, *120*, 10145.
[5] M. Li, Y. F. Wang, D. Zhang, L. Duan, C. F. Chen, *Angew. Chem., Int. Ed.* **2020**, *59*, 3500.
[6] J. Han, S. Guo, J. Wang, L. Wei, Y. Zhuang, S. Liu, Q. Zhao, X. Zhang, W. Huang, *Adv. Opt. Mater.* **2017**, *5*, 1700359.
[7] C. Wagenknecht, C. M. Li, A. Reingruber, X. H. Bao, A. Goebel, Y. A. Chen, Q. Zhang, K. Chen, J. W. Pan, *Nat. Photonics* **2010**, *4*, 549.
[8] Y. Yang, R. C. da Costa, M. J. Fuchter, A. J. Campbell, *Nat. Photonics* **2013**, *7*, 634.
[9] M. R. Craig, P. Jonkheijm, S. C. J. Meskers, A. P. H. J. Schenning, E. W. Meijer, *Adv. Mater.* **2003**, *15*, 1435.
[10] B. Langeveld-Voss, R. Janssen, M. Christiaans, S. Meskers, H. Dekkers, E. Meijer, *J. Am. Chem. Soc.* **1996**, *118*, 4908.
[11] G. Albano, L. A. Aronica, A. Minotto, F. Cacialli, L. D. Bari, *Chem. - Eur. J.* **2020**, *26*, 16622.
[12] L. Wan, J. Wade, X. Shi, S. Xu, M. J. Fuchter, A. J. Campbell, *ACS Appl. Mater. Interfaces* **2020**, *12*, 39471.
[13] L. Frédéric, A. Desmarchelier, R. Plais, L. Lavnevich, G. Muller, C. Villafuerte, G. Clavier, E. Quesnel, B. Racine, S. Meunier-Della-Gatta, J.-P. Dognon, P. Thuéry, J. Crassous, L. Favereau, G. Pieters, *Adv. Funct. Mater.* **2020**, *30*, 2004838.
[14] S. Chen, D. Katsis, A. Schmid, J. Mastrangelo, T. Tsutsui, T. Blanton, *Nature* **1999**, *397*, 506.
[15] D. M. Lee, J. W. Song, Y. J. Lee, C. J. Yu, J. H. Kim, *Adv. Mater.* **2017**, *29*, 1700907.
[16] K. Baek, D. M. Lee, Y. J. Lee, H. Choi, J. Seo, I. Kang, C. J. Yu, J. H. Kim, *Light: Sci. Appl.* **2019**, *8*, 120.
[17] T. Sugiyama, Y. Toko, T. Hashimoto, K. Katoh, Y. Iimura, S. Kobayashi, *Jpn. J. Appl. Phys.* **1993**, *32*, 5621.
[18] P. G. de Gennes, J. Prost, *The Physics of Liquid Crystals*, 2nd ed., Oxford University Press, Oxford **1993**.
[19] J. H. Jung, D. M. Lee, J. H. Kim, C. J. Yu, *J. Mater. Chem. C* **2018**, *6*, 726.
[20] S. I. Jo, Y. Kim, J. H. Baek, C. J. Yu, J. H. Kim, *Jpn. J. Appl. Phys.* **2014**, *53*, 03CD04.
[21] K. S. Whitehead, M. Grell, D. D. C. Bradley, M. Jandke, P. Strohriegl, *Appl. Phys. Lett.* **2000**, *76*, 2946.
[22] M. Grell, D. D. Bradley, M. Inbasekaran, E. P. Woo, *Adv. Mater.* **1997**, *9*, 798.
[23] M. Hamaguchi, K. Yoshino, *Appl. Phys. Lett.* **1995**, *67*, 3381.
[24] Y. Zhou, Z. He, S. Sato, *Jpn. J. Appl. Phys.* **1999**, *38*, 4857.
[25] Y. Zhou, Z. He, S. Sato, *Jpn. J. Appl. Phys.* **1997**, *36*, 2760.
[26] M. Jiang, Z. Wang, R. Sun, K. Ma, R. Ma, X. Huang, *Jpn. J. Appl. Phys.* **1994**, *33*, L1242.
[27] B. R. Acharya, J.-H. Kim, S. Kumar, *Phys. Rev. E* **1999**, *60*, 6841.
[28] G. Albano, M. Górecki, G. Pescitelli, L. D. Bari, T. Jávorfi, R. Hussain, G. Siligardi, *New J. Chem.* **2019**, *43*, 14584.
[29] S. K. So, W. K. Choi, L. M. Leung, K. Neyts, *Appl. Phys. Lett.* **1999**, *74*, 1939.
[30] T. Granlund, L. A. A. Pettersson, O. Inganäs, *J. Appl. Phys.* **2001**, *89*, 5897.
[31] F. Zinna, M. Pasini, F. Galeotti, C. Botta, L. Di Bari, U. Giovanella, *Adv. Funct. Mater.* **2017**, *27*, 1603719.